Ceramics International (xxxx) xxxx–xxxx

Contents lists available at ScienceDirect

Ceramics International

journal homepage: www.elsevier.com/locate/ceramint

Short communication

Facile synthesis of lithium-vanadium-molybdenum oxide nanocomposite as high-performance anode material for lithium ion batteries

Qingmei Zhao[a,*], Wenliang Li[b], Wei Xiao[a], Wenjie Peng[b,*], Xuemin Yan[a], Chang Miao[a]

[a] College of Chemistry and Environmental Engineering, Yangtze University, Jingzhou 434023, China
[b] School of Metallurgy and Environment, Central South University, Changsha 410083, China

ARTICLE INFO

Keywords:
Lithium ion battery
Lithium-vanadium-molybdenum oxide
Nanocomposites
Mechanical activation
Energy storage and conversion

ABSTRACT

A lithium-vanadium-molybdenum-oxide composite has been prepared by a soft chemical route with mechanical activation assistance followed by low-temperature heat treatment in argon atmosphere. The X-ray diffraction reveals that the synthesized sample is made up of $Li_3V(MoO_4)_3$ and $LiVOMoO_4$ crystal phases. The SEM images show the fine particles ~300 nm in size. HRTEM image shows a clear crystal boundary between the two phases. The composite possesses good electrochemical performance as anode material. Particularly, it delivers an initial charge capacity of 927 mAh g^{-1} at 50 mA g^{-1} with a high initial coulombic efficiency of 81.2% and maintains 87.8% of its initial capacity after 50 cycles. Even if tested at 1000 mA g^{-1}, it can deliver a reversible capacity of 542 mA h g^{-1}.

1. Introduction

Lithium ion battery (LIB) is one of the most important energy-storage devices because of its high energy density and good design flexibility.[1–5] As one of the important components of LIBs, the anode material has an overriding influence on the performance of LIBs.[6–8] The graphite has become the most common commercial anode.[9–11] However, the graphite suffers from many problems, such as low theoretical capacity (372 mA h g^{-1}), low Li^+ diffusion coefficient and serious safety issues.[12,13] Therefore, it is necessary to explore new and utility anode materials for LIBs.[14] Recently, the complex polyanionic molybdates, such as $LiFe(MoO_4)_2$[15] and $Li_2Ni_2(MoO_4)_3$[16], are considered as the promising intercalation-type materials for lithium ion storage because of the structural stability and significant Li-ion mobility.[17] Among these materials, lithium vanadium molybdate, $Li_3V(MoO_4)_3$, was proposed as a novel mixed molybdenum-vanadium oxide with an orthorhombic structure and large channels half-filled with Li atoms.[18] It is found that $Li_3V(MoO_4)_3$ shows the Li^+ insertion/extraction ability at the potential window from 1.4 to 4.9 V, delivering a specific capacity of ~120 mA h g^{-1}. Interestingly, considering the various oxidation states of V and Mo, it is expected that $Li_3V(MoO_4)_3$ has the ability to deliver a high specific capacity at a low voltage window. In addition, Composite of two or more materials can improve the electrochemical performance of the material because of the synergistic effect. [19,20].

Herein, for the first time, we introduce a facile method to prepare lithium-vanadium-molybdenum-oxide composite ($Li_3V(MoO_4)_3$@ $LiVOMoO_4$). It is synthesized via one-step soft chemical route with mechanical activation assistance followed by low-temperature heat treatment. The lithium storage capacity of this composite is evaluated at the potential window of 0.01–3.0 V.

2. Experimental

Firstly, the stoichiometric V_2O_5, CH_3COOLi, $(NH_4)_6Mo_7O_{24}$ and oxalic acid (10 wt% excess) were mixed by grinding in an agate mortar. Secondly, the mixture was dispersed into alcohol to form the homogeneous slurry and poured into the goal grinding jar. Thirdly, the slurry reacted under high-energy ball milling (ND6–2 L, 0.75 kW) for 8 h with a revolving speed of 200 r min^{-1}. After that, the obtained light yellow slurry was dried in the vacuum oven at 120 °C for overnight. Finally, the obtained precursor was sintered at 300 °C for 3 h and then annealed at 600 °C for 10 h in a tube furnace under argon atmosphere.

The powder X-ray diffraction (XRD, Rint-2000, Rigaku) using Cu Kα radiation was employed to examine the crystalline phase of the synthesized composite. Field emission scanning electron microscope (FESEM, Hitachi S4800, 20 kV) and transmission electron microscopy (TEM, Titan G2 60–300 with image corrector) were carried out to observe the morphology of the obtained sample. The elemental distributions in the prepared composite were evaluated by energy dispersive spectrometer (EDS) mapping analysis.

The electrochemical performance of the prepared composite was

* Corresponding authors.
E-mail addresses: qingmeizhao123@163.com (Q. Zhao), pwj_csu@163.com (W. Peng).

http://dx.doi.org/10.1016/j.ceramint.2016.12.011
Received 30 November 2016; Received in revised form 2 December 2016; Accepted 2 December 2016

evaluated in CR2025 coin-type cells. To fabricate the working electrodes, 10 wt% of conductive agent (acetylene black), 10 wt% of blinder (polyvinylidene fluoride) and 80 wt% of as-prepared active material were mixed into the N-methyl pyrrolidinone (NMP) to form the slurry. After that, the slurry was pasted on a copper foil, followed by drying at 120 °C for 6 h in an oven. The dried electrodes were punched in the form of 12 mm diameter disks. The cells were assembled in a dry argon-filled glove box. The lithium foil was used as the counter electrode. A porous polypropylene film was employed as the separator. The electrolyte was 1 mol L^{-1} $LiPF_6$ in EC/EMC/DMC (1:1:1 in volume). The electrochemical tests were carried out by NEWARE battery circler, between 0.01 V and 3.0 vs. Li^+/Li at room temperature. The electrochemical analyzer (CHI660A) was used to conduct the electrochemical impedance spectroscopy (EIS) and cyclic voltammetry (CV) measurements. CV test was carried out in the voltage range of 0.01–3.0 V vs. Li^+/Li electrode at a scanning rate of 0.05 mV s^{-1}. The impedance spectra were recorded by applying an AC voltage of 5 mV amplitude in the frequency range of 0.01 Hz–100 kHz.

3. Results and discussion

As shown in Fig. 1(a), the high-intensity XRD peaks can be indexed with $Li_3V(MoO_4)_3$ [marked with "•"] and $LiVOMoO_4$ [marked with "×"], indicating that this composite is made up of orthorhombic $Li_3V(MoO_4)_3$ and brannerite-type $LiVOMoO_4$. In addition, there is no peak corresponding to the added oxalic acid. This is because that the oxalic acid is changed to amorphous carbon during the annealing process. The HRTEM image in Fig. 1(b) shows different lattices between area "1" and "2". The corresponding IFFT images taken from area "1" and "2" are shown in Fig. 1(c) and (d), respectively. Fig. 1(c) shows a lattice fringe spacing of 0.2693 nm that can be indexed with (051) lattice plane of $LiVOMoO_4$. However, Fig. 1(d) shows a lattice fringe spacing of 0.1787 nm that can be indexed with (226) lattice plane of $Li_3V(MoO_4)_3$. Therefore, the HRTEM results confirm that the $Li_3V(MoO_4)_3$ and $LiVOMoO_4$ crystals inset into each other in the composite. It has been reported that composites of two or more materials can improve the conductivity of the materials because of the synergistic effect of each component.[19,20].

The SEM images of the composite in Fig. 2(a) and (b) show the agglomerations of primary nano-sized particles (200–400 nm) with a clean and smooth surface. There are many pores between the particles, which are beneficial to the charge transfer of composite electrode during the cycling process. EDS result in Fig. 2(c) demonstrates that the Mo/V ratio in the composite is almost the same as that in raw materials. In addition, the carbon content is about 2.18 wt%. The carbon is derived from oxalic acid decomposition and is in favor of electronic conductivity of the as-prepared composite. The EDS mappings [Fig. 2(d–f)] show that elements Mo, V are homogeneously distributed in the particles.

The CV curves of composite are presented in Fig. 3(a). During negative scanning in the first cycle, the composite electrode experiences a reductive peak at around 1.7 vs. Li^+/Li that is associated with the V^{+3}/V^{+2} redox. At the low voltage, an intensive peak is found, which is corresponded to the typical conversion reaction accompanying with electrolyte decomposition and solid-electrolyte-interface (SEI) film formation. When the first cycle completes, the reaction becomes stable and the following curves are overlapped. This indicates that the cell possesses low polarization and good reversibility.Fig. 3(b) shows the galvanostatic charge–discharge profiles of the prepared composite in the potential range of 3.0–0.01 V at different current densities. It can be seen that the first discharge curve exhibits a lithiation plateau at ~1.65 V that is related to the reduction of V^{3+} to V^{2+}, which is consistent with CV curves. Two long plateaus at around 0.6 V and 0.3 V are also found in the discharge curve, indicating that the prepared composite can be used as a promising anode material with high capacity. At a current density of 50 mA g^{-1}, the composite electrode delivers an initial discharge and charge capacity of 1141 and 927 mA h g^{-1}, respectively. As a result, the coulombic efficiency is 81.2%, which is much larger than that of other transition metal oxides as reported.[1,6,21] The sample shows good rate capability. The reversible capacities are 819, 674 and 542 mA h g^{-1} at 100, 500 and 1000 mA g^{-1}, respectively. It can be seen from Fig. 3(c) that the composite electrode also possesses good cycle performance, maintaining 87.8%, 74.5% and 66.6% capacity retention after 50 cycles at 50, 500 and 1000 mA g^{-1}, respectively. The EIS curve of the sample after 2 cycles at 3.0 V is shown in Fig. 3(d). It exhibits a profile that is composed of a semi-circle in the high-to-medium frequency region and a straight line in the low-frequency region. The semicircle is corresponded to charge transfer impedance (R_{ct}//CPE_{dl}). The sloping line in the lower frequency region is indexed with the semi-infinite diffusion of lithium-ion (W_o). The impedance spectra are fitted by the equivalent electrical circuit as shown in Fig. 3(d). Of particular note is that the R_{ct} value of prepared sample is very small (~65 Ω), reflecting the composite electrode delivers the fast charge transfer mobility. Based on the linear relationship between the reciprocal square root of the angular frequency ($\omega^{-1/2}$) and real axis (Z_{re}) in the Warburg region, the lithium ion diffusion efficient can be calculated based on the following Eqs. (1) and (2):

$$Z_{re}=R_e+R_{ct}+\sigma_\omega\omega^{1/2} \quad (1)$$

$$D_{Li^+} = 0.5(RT/AF^2\sigma_\omega C_{Li^+})^2 \quad (2)$$

Whereas A is the electrode area (1.13 cm^2); C_{Li^+} is the lithium concentration in the composite (herein ~1.0×10^{-2} mol cm^{-3}). Based on these, the calculated D_{Li^+} is about 2.07×10^{-13} cm^2 s^{-1}. It suggests the prepared $Li_3V(MoO_4)_3$@$LiVOMoO_4$ composite is an good anode material for lithium ion batteries.

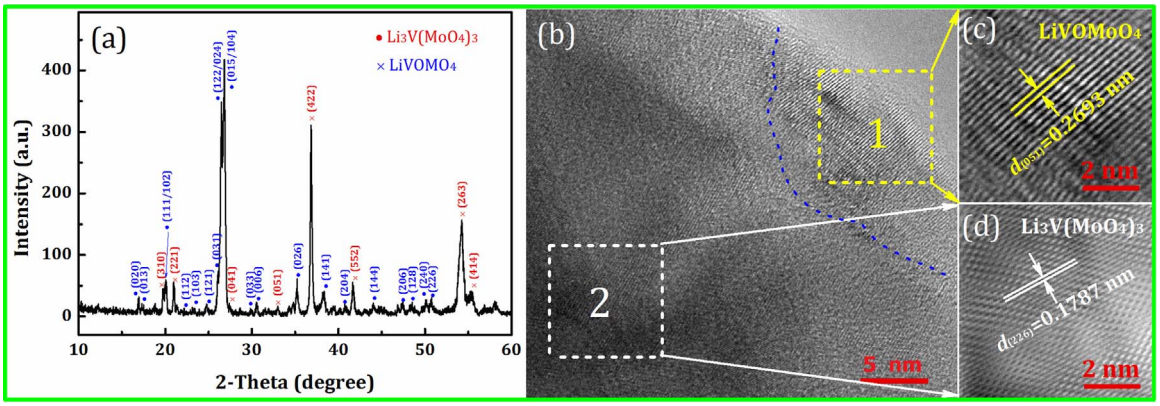

Fig. 1. (a) XRD pattern, (b) HRTEM and (c, d) IFFT images of the as-prepared composite.